A Novel Sensing and Symbiotic Communication Approach

Thai-Hoc Vu, Anh-Tu Le, Lam-Thanh Tu, *Member, IEEE*, Nguyen Cong Luong, and Miroslav Voznak, *Senior Member, IEEE*

***Abstract*—As next-generation technologies promise seamless integration of sensing and communication within unified systems by leveraging shared frequencies, signaling, and hardware, it is of interest to explore new communication approaches in a reciprocal and symbiotic manner. This letter proposes a sensing and symbiotic communication (SaSC) approach for uplink scenarios, where the base station simultaneously performs radar sensing, user communication, and backscatter information collection. To enforce symbiotic communications efficiently, adaptive reflective coefficients for backscatter nodes and diversity techniques for user communication receptions are jointly established. Upon this, closed-form expressions are derived to quantify outage probability for symbiotic communication and mutual information for radar sensing. Besides, deep quantitative analyses of high transmit power regimes and low rates are also analyzed to attain insights into system designs and solve a non-convex problem of the radar transmit power optimization to maximize radar mutual information under throughput constraints of symbiotic communication. Moreover, to achieve mutual interference cancellation between radar and symbiotic communication signals, a model of reversed radar symbols over consecutive periods has been outlined as a benchmark scheme. Simulation results affirm the potential and effectiveness of the proposed SaSC approach.**

***Index Terms*—Sensing and symbiotic communication (SaSC), performance analysis, radar mutual information, uplink sensing.**

I. Introduction

As MOBILE and Internet-of-Things (IoT) devices proliferate in communication networks, the urgency of addressing the demands of both communication and radar systems, without enlarging current spectrum resources, has never been more pressing. In light of this, an exciting wave of research is turning its attention to the innovative use of shared time-frequency resources for both sensing and communication, known as integrated sensing and communication (ISaC) [1].

Received 17 June 2025; accepted 3 December 2025. Date of publication 9 December 2025; date of current version 26 December 2025. This work was supported in part by the European Union under the REFRESH—Research Excellence for Region Sustainability and High-Tech Industries Project through the Operational Programme Just Transition under Grant CZ.10.03.01/00/22_003/0000048, and in part by the Ministry of Education, Youth and Sports of the Czech Republic (MEYS CZ) within a Student Grant Competition in the VSB—Technical University of Ostrava under Project SGS SP2025/013. The associate editor coordinating the review of this article and approving it for publication was H. Xing. *(Corresponding author: Lam-Thanh Tu.)*

Thai-Hoc Vu, Anh-Tu Le, and Miroslav Voznak are with the Faculty of Electrical Engineering and Computer Science, VSB-Technical University of Ostrava, 708 00 Ostrava, Czechia (e-mail: thai.hoc.vu@vsb.cz; anh.tu.le@vsb.cz; miroslav.voznak@vsb.cz).

Lam-Thanh Tu is with the Advanced Intelligent Technology Research Group, Faculty of Electrical and Electronics Engineering, Ton Duc Thang University, Ho Chi Minh City 70000, Vietnam (e-mail: tulamthanh@tdtu.edu.vn).

Nguyen Cong Luong is with the Phenikaa School of Computing, Phenikaa University, Hanoi 12116, Vietnam (e-mail: luong.nguyencong@phenikaa-uni.edu.vn).

Digital Object Identifier 10.1109/LWC.2025.3641971

ISaC bridges the gap between sensing and communication, sparking a large body of research in the literature. For a review, please refer to [2] and the in-depth discussions therein. Yet, it is noteworthy that most ISaC studies focus on angle of arrival/departure estimators, waveform designs, and beamforming techniques (e.g., [3], [4]), with less attention given to fundamental performance metrics (i.e., [5], [6]). Notably, recent advancements have integrated ISaC with symbiotic radio (SR) technologies, resulting in a symbiotic sensing and communication (SSaC) paradigm [7]. This stimulates secondary devices, namely backscatter devices (BDs), to cooperate with primary networks to achieve cost-effective deployment and multipath gains for enhanced functionalities like object detection and localization.

On this foundation, Hakimi et al. [8] proposed enhancing primary communication and enable secondary backscatter data transmission by an ISaC-SR-based reconfigurable intelligent surface system, focusing on maximizing sum rate through jointly optimizing full-duplex base station (BS) beamformers and reconfigurable phase shifts. Meanwhile, Tao *et al.* tackled the challenges associated with limited channel information by developing a 2D angle-of-arrival estimator for mobile ISaC-SR scenarios [9] and an advanced Bayesian learning algorithm for IoT device identification in ISaC-aided IoT networks [10]. Additionally, Xia et al. in [11] outlined an SSaC framework, where the BS serves vehicle users while a sensing node conducts bistatic sensing and shares these results with the BS to support fully digital or hybrid beamforming designs.

The literature reviewed highlights that previous works [8], [9], [10], [11] have laid the groundwork for integrating ISaC into SR systems. However, the impact of adaptive symbiotic communication (SymCom) in backscattering IoT systems has not been touched, and these studies lack insights into system designs like diversity order. Specifically, the convergence of radar sensing and SymCom (SaSC) for achieving user equipment (UE) communication, backscattering data collection, and radar target (RT) detection has not been explored.

To fulfill this letter gap, we propose a mathematical framework for evaluating uplink SaSC systems, where a BS senses one RT while communicating with its UE and a BD. Our approach includes a joint design for the adaptive backscatter coefficient at the BD and two antenna diversity techniques: selection combining (SC) and beamforming-based maximal ratio combining (MRC). We derive exact expressions for outage probability (OP) metrics for SymComs and radar mutual information for radar sensing. Additionally, we tackle the non-convex optimization of radar transmission power to enhance radar detection while meeting throughput of SymCom conditions. We also present an auto-canceling radar signal model to boost adaptive SymCom performance, laying the basis for comparative purposes.

II. System Model Description

In an SaSC shown in Fig. 1, one BS receives symbiotic data communication from one UE and one BD capable of signal processing. Meanwhile, the BE senses an RT based on radar signal reflection. The BS operates in full-duplex mode [5] through two distinct sets of spatially separated antennas: one array comprising L-antennas dedicated to SymCom and a single antenna designated for radar function.

Let us denote by $h_{\rm c}$ the channel from UE to BS. $h_{\rm b}$ is the backscatter channel, which is cascaded by the channels from UE to BD, denoted by g_u, and from BD to BS, denoted by g_b, such that $h_{\rm b} = g_u g_b$. $h_{\rm r}$ is the two-way radar channel from BS to RT and from RT to BS. In this letter, we model $h_{\rm c}$, g_u, g_b, and $h_{\rm r}$ as complex Gaussian random variables with zero-mean and the corresponding variance $\Omega_{\rm c} = \mathbb{E}\{|h_{\rm c}|^2\}$, $\Omega_{\rm u} = \mathbb{E}\{|g_u|^2\}$, $\Omega_{\rm b} = \mathbb{E}\{|g_b|^2\}$, and $\Omega_{\rm r} = \mathbb{E}\{|h_{\rm r}|^2\}$. More specific modeling of these variances under the pathloss effects for communications and radar signals can be found in [3].

For the sake of notation, we denote by $\mathcal{L} = \{1, 2, \ldots, L\}$ a set of the receiving antenna at BS. $x_{\rm c}$, $x_{\rm b}$, and $x_{\rm r}$ are the normalized UE signal, backscatter message, and radar impulse, respectively, with $\mathbb{E}\{|x_{\rm c}|\} = \mathbb{E}\{|x_{\rm b}|\} = \mathbb{E}\{|x_{\rm r}|\} = 0$ and $\mathbb{E}\{|x_{\rm c}|^2\} = \mathbb{E}\{|x_{\rm b}|^2\} = \mathbb{E}\{|x_{\rm r}|^2\} = 1$. Under a single antenna reception, the received signal at BS can be given by

$$y = \sqrt{p_{\rm u}} h_{\rm c} x_{\rm c} + \sqrt{\beta} x_{\rm b} \sqrt{p_{\rm u}} h_{\rm b} x_{\rm c} + \sqrt{p_{\rm s}} h_{\rm r} x_{\rm r} + n, \quad (1)$$

where $p_{\rm u}$ is the UE's transmit power, $\beta > 0$ is a backscattering coefficient, $p_{\rm s}$ is the BS's transmit power for the radar function, and n is the Gaussian noise with zero mean and variance N_0.

To strengthen communication signal reception, we consider the SC technique to select the strongest signal path for UE-BS links, which yields $X_1 \triangleq \max_{l\in\mathcal{L}} |h_{\rm c}^l|^2$, and the beamforming-based MRC strategy with the weight $\boldsymbol{w} = \boldsymbol{h}_{\rm c}^H / \|\boldsymbol{h}_{\rm c}\|$, which leads to $X_2 \triangleq \|\boldsymbol{h}_{\rm c}\|^2$. Since the quality of the main communication channel gains $X \in \{X_1, X_2\}$ is stronger than those of cascaded channels, including $Y \triangleq |h_{\rm b}|^2$ and $Z \triangleq |h_{\rm r}|^2$, BS decodes $x_{\rm c}$ first, followed by $x_{\rm b}$, and finally estimating $x_{\rm r}$. Combining this with (1), the minimal signal-to-interference-plus-noise ratio (SINR) for decoding $x_{\rm c}$ and $x_{\rm b}$ are given by

$$\gamma = \min\left\{ \frac{p_{\rm u} X}{\beta p_{\rm u} Y + p_{\rm s} Z + N_0}, \frac{\beta p_{\rm u} Y}{p_{\rm s} Z + N_0} \right\}. \quad (2)$$

III. Performance Analysis

A. Symbiotic Communication Analysis: Outage Probability

The outage event occurs whenever the achievable rate $C(\gamma) = \log_2(1+\gamma)$ in bps/Hz, with the SINR given in (2), falls below the minimal target data rate R_m in bps/Hz. Henceforth, the outage probability can be mathematically derived as

$$\text{OP} = \Pr(C(\gamma) \le R_m) = F_\gamma\left(2^{R_m} - 1\right), \quad (3)$$

where $F_\gamma(\bullet)$ is the cumulative distribution function (CDF) of γ. From (3), it is evident that minimizing OP is equivalent to maximizing γ. Let $f_1(\beta) = p_{\rm u} X / (\beta p_{\rm u} Y + \Delta)$, and $f_2(\beta) = \beta p_{\rm u} Y / \Delta$, where $\Delta \triangleq p_{\rm s} Z + N_0$. We have the following.

Observation 1: It is safe to conclude that $f_1(\beta)$ is a decreasing function of β while $f_2(\beta)$ is an increasing function of β.

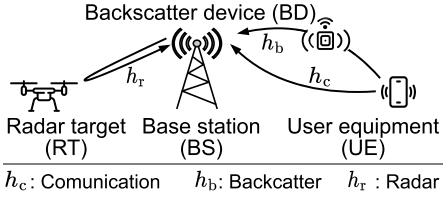

Fig. 1. Illustration of the proposed SaSC system.

Proof: This observation is obtained by taking derivatives of $f_1(\beta), f_2(\beta)$ with respect to β, which yields $f_1'(\beta) = -p_{\rm u} X p_{\rm u} Y / (\beta p_{\rm u} Y + \Delta)^2 < 0$ and $f_2'(\beta) = p_{\rm u} Y / \Delta > 0$. ■

Observation 1 states that γ becomes maximal if and only if $f_1(\beta) = f_2(\beta)$. From this, we have the following proposition.

Proposition 1: The optimal value of β for minimizing the OP and the optimal SINR of γ can be determined, respectively, as

$$\beta^\star = \frac{\sqrt{\Delta^2 + 4 p_{\rm u} X \Delta} - \Delta}{2 p_{\rm u} Y}, \gamma^\star = \frac{\sqrt{1 + 4 p_{\rm u} X / \Delta} - 1}{2}. \quad (4)$$

Proof: By solving $f_1(\beta) = f_2(\beta)$, we get that

$$(p_{\rm u} Y)^2 \beta^2 + p_{\rm u} Y (p_{\rm s} Z + N_0)\beta - p_{\rm u} X (p_{\rm s} Z + N_0) = 0$$
$$\Leftrightarrow \beta = \left(\pm\sqrt{\Delta^2 + 4 p_{\rm u} X \Delta} - \Delta\right) / (2 p_{\rm u} Y). \quad (5)$$

Since $\beta > 0$, only positive root is valid. Next, injecting this root into $f_2(\beta)$ yields the optimal SINR, ending the proof. ■

Upon this proposition, we can derive the CDF of $\gamma^\star$ as

$$F_{\gamma^\star}(x) = \Pr(\gamma^\star < x) = \Pr\left(4 p_{\rm u} X < \Delta\left[(2x+1)^2 - 1\right]\right)$$
$$= \int_0^\infty F_X\left((p_{\rm s} z + N_0)\left(x^2 + x\right) / p_{\rm u}\right) f_Z(z) dz. \quad (6)$$

To derive (6), it is required to determine the CDF of X as

$$F_X(x) = \begin{cases} [1 - \exp(-x/\Omega_{\rm c})]^L, & X = X_1, \quad (7a) \\ 1 - \Gamma(L, x/\Omega_{\rm c})/\Gamma(L), & X = X_2, \quad (7b) \end{cases}$$

where $\Gamma(\bullet, \bullet)$ is the upper incomplete Gamma function [12, (8.350.2)]. The probability density function of Z is given by

$$f_Z(z) = \exp(-z/\Omega_{\rm r})/\Omega_{\rm r}. \quad (8)$$

Injecting (7) and (8) into (6) along with the aid of Appendix A and denoting $\theta = \frac{p_{\rm s}\Omega_{\rm r}}{p_{\rm u}\Omega_{\rm c}}$, we get the following lemma.

Lemma 1: The CDF of $\gamma^\star$ can be calculated as in (9), shown at the bottom of the next page.

To collect more insights, we turn to analyze the scenario when $p_{\rm u}$ becomes large enough or R_m is set to be small.

Corollary 1: Given a sufficient large non-negative value x, the optimal CDF of $\gamma^\star$ behaves asymptotic as

$$F_{\gamma^\star}(x) \approx \begin{cases} [(x^2 + x)/(p_{\rm u}\Omega_{\rm c})]^L \Phi, & X = X_1, \quad (10a) \\ \dfrac{[(x^2 + x)/(p_{\rm u}\Omega_{\rm c})]^L \Phi}{\Gamma(L+1)}, & X = X_2, \quad (10b) \end{cases}$$

where $\Phi \triangleq \sum_{l=0}^{L} \binom{L}{l} (p_{\rm s}\Omega_{\rm r})^l (N_0)^{L-l} \Gamma(l+1)$.

Proof: Applying the infinitesimal equivalent $1 - \exp(-x) \simeq x$ as $x \to 0$ and the first order of Taylor series expansion in [12, 8.354], the result in (7) can be approximated as

$$F_X(x) \overset{x\to 0}{\simeq} \begin{cases} (x/\Omega_{\rm c})^L, & X = X_1, \quad (11a) \\ (x/\Omega_{\rm c})^L / \Gamma(L+1), & X = X_2. \quad (11b) \end{cases}$$

Next, by injecting (11) and (8) into (6) before applying the identity in [12, (1.111)] to decompose $(p_{\rm s}z+N_0)^L$ into $\sum_{l=0}^{L}\binom{L}{l}(p_{\rm s})^l(N_0)^{L-l}z^l$, the results of $F_{\gamma^\star}(x)$ with (11a) and (11) then have the same integral form $\int_0^\infty z^l\exp(-z/\Omega_{\rm r})dz$, which can be solved using [12, (3.326.2)]. ■

Remark 1: Some insights can be drawn from (10) and (3) as follows. **First**, dividing (10) to (10a) shows that employing beamforming-based MRC strategy can improve the OP by $\Gamma(L+1)$ times over the SC approach. **Second**, both diversity approaches have the same diversity order L because the optimal OP is proportional to $F_{\gamma^\star}(x)$, which scales with $1/p_{\rm u}^L$. **Third**, increasing the minimum target rate R_m increases the outage event, which is because $F_{\gamma^\star}(x)$ scales with (x^2+x). **Fourth**, the OP is decreased with a increase the BS's transmit power $p_{\rm s}$ for radar sensing due to the increase of Φ in $F_{\gamma^\star}(x)$.

B. Radar Sensing Analysis

1) Mutual Information Analysis: After decoding the communication signal and backscattering message and removing these signals from (1), the radar signal can be given by $y_{\rm rad}=\sqrt{p_{\rm s}}h_{\rm r}x_{\rm r}+n$. Then, the radar mutual information over the whole time of communication can be derived as

$$I_{\rm rad}=I(h_{\rm r};y_{\rm rad})=B\,\mathbb{E}\{\log_2(1+p_{\rm s}Z/N_0)\}. \tag{12}$$

where $I(X;Y)$ denotes the mutual information and B is the denotes the bandwidth (MHz). From (8), (12) is rewritten as

$$\begin{aligned}I_{\rm rad}&=\frac{B}{\ln(2)}\int_0^\infty \ln(1+zp_{\rm s}/N_0)f_Z(z)dz\\&=-\frac{B}{\ln(2)}\frac{\mathrm{Ei}(-N_0/\Omega_{\rm r}/p_{\rm s})}{\exp(-N_0/\Omega_{\rm r}/p_{\rm s})}\triangleq\psi(p_{\rm s}),\end{aligned} \tag{13}$$

which is derived using [12, (4.337.2)] and $\mathrm{Ei}(\bullet)$ is the exponential integral function [12, (8.211.1)].

2) Optimization Problem: Our next objective is to improve radar performance by adjusting $p_{\rm s}$, while maintaining the throughput $\mathcal{R}=B\,\mathbb{E}\{\log_2(1+\gamma^\star)\}$ in Mbps with the optimal SINR $\gamma^\star$ for SymCom performance provided in (4) remains above the communication threshold $\mathcal{R}_{th}$ [Mbps], i.e.,

$$\max_{p_{\rm s}}\quad I_{\rm rad}\quad\text{s.t.}\quad\mathcal{R}\geq\mathcal{R}_{th}. \tag{14}$$

The non-convexity of Problem (14) arises from the nonlinear objective and logarithmic constraints. Additionally, a huge effort in deriving the closed-form solution for the throughput $\mathcal{R}$ alongside the involvement of special functions in the mutual information formula in (13) makes this optimization problem highly challenging to solve.

Solution Approach: To overcome such a challenge, we first apply successive convex approximation (SCA) method to handle the non-convexity of the objective function in (13) by introducing the following inequality for a function $f(x)=\log_2(1+x)$ with $x>0$ at local point $\overline{x}>0$ as

$$f(x)\geq f(\bar{x})+\frac{\bar{x}^2(1/\bar{x}-1/x)}{\ln(2)(\bar{x}+1)}, \tag{15}$$

which is derived using Taylor series for $f(1/y)$ before mapping $x=1/y$. Upon this, we map $x=p_{\rm s}Z/N_0$ and $\bar{x}=\bar{p}_{\rm s}Z/N_0$ to rewrite $I_{\rm rad}$ in (12) by a concave form as

$$\begin{aligned}I_{\rm rad}&\geq B\times\mathbb{E}\left\{\log_2\left(1+\frac{\bar{p}_{\rm s}Z}{N_0}\right)+\frac{\bar{p}_{\rm s}Z\left(1-\frac{\bar{p}_{\rm s}}{p_{\rm s}}\right)}{\ln(2)(N_0+\bar{p}_{\rm s}Z)}\right\}\\&=\psi(\bar{p}_{\rm s})+B\times\frac{\bar{p}_{\rm s}\mathbb{E}\{Z\}(1-\bar{p}_{\rm s}/p_{\rm s})}{\ln(2)(N_0+\bar{p}_{\rm s}\mathbb{E}\{Z\})},\end{aligned} \tag{16}$$

where $\mathbb{E}\{Z\}=\Omega_{\rm r}$. Next, we handle the constrain in (14) by introducing the following inequality for a function $g(x)=\log_2(1+\sqrt{1+c/x})$ with $x,c>0$ at local point $\overline{x}>0$ as

$$g(x)\geq g(\bar{x})+\frac{(2-x/\bar{x}-(\bar{x}+c)/(x+c))}{2\ln(2)\left(1+\sqrt{\bar{x}/(\bar{x}+c)}\right)}. \tag{17}$$

The proof of (17) is provided in Appendix B. By mapping $c=4p_{\rm u}X$, $x=p_{\rm s}Z+N_0$ and $\bar{x}=\bar{p}_{\rm s}Z+N_0$, we can approximate $\mathcal{R}$ by an equivalent concave form as

$$\begin{aligned}\mathcal{R}\;&\geq B\times\mathbb{E}\{\log_2\left(1+\sqrt{1+4p_{\rm u}X/(\bar{p}_{\rm s}Z+N_0)}\right)\}-B\\&+\frac{B\times\left(2-\frac{p_{\rm s}\mathbb{E}\{Z\}+N_0}{\bar{p}_{\rm s}\mathbb{E}\{Z\}+N_0}-\frac{\bar{p}_{\rm s}\mathbb{E}\{Z\}+N_0+4p_{\rm u}\mathbb{E}\{X\}}{p_{\rm s}\mathbb{E}\{Z\}+N_0+4p_{\rm u}\mathbb{E}\{X\}}\right)}{2\ln(2)\left(1+1/\mathbb{E}\{\sqrt{1+4p_{\rm u}X/(\bar{p}_{\rm s}Z+N_0)}\}\right)},\end{aligned} \tag{18}$$

where $\wp\triangleq\mathbb{E}\{X\}=\int_0^\infty[1-F_X(x)]dx$, $\Xi(\bar{p}_{\rm s})\triangleq\mathbb{E}\{\log_2(1+U)\}=\int_0^\infty\frac{1-F_U(u)}{\ln(2)(1+u)}du$, and $\chi(\bar{p}_{\rm s})\triangleq\mathbb{E}\{U\}=\int_0^\infty[1-F_U(u)]du$, with $U=\sqrt{1+4p_{\rm u}X/(\bar{p}_{\rm s}Z+N_0)}$.

Making use of (7) and [12, (3.326.2)], we get that

$$\wp=\begin{cases}\sum_{l\in\mathcal{L}}\binom{L}{l}(-1)^{l-1}\Omega_{\rm c}/l, & X=X_1, \quad (19a)\\ L\Omega_{\rm c}, & X=X_2. \quad (19b)\end{cases}$$

Meanwhile, we use Appendix C to respectively derive $\Xi(\bar{p}_{\rm s})$ and $\chi(\bar{p}_{\rm s})$ as in (20), shown at the bottom of the next page and (21), where K is the trade-off parameter, $\phi_k=\cos((2k-1)\pi/[2K])$, and $\tau_k=(\phi_k+3)/4$.

Putting all together, we can convert the problem in (14) into an convex approximation one to be solved using CVX tools:

$$\max_{p_{\rm s}}\ \psi(\bar{p}_{\rm s})+B\times\frac{\bar{p}_{\rm s}\Omega_{\rm r}(1-\bar{p}_{\rm s}/p_{\rm s})}{\ln(2)(N_0+\bar{p}_{\rm s}\Omega_{\rm r})} \tag{22a}$$

$$\text{s.t.}\quad\Xi(\bar{p}_{\rm s})+\frac{2-\frac{p_{\rm s}\Omega_{\rm r}+N_0}{\bar{p}_{\rm s}\Omega_{\rm r}+N_0}-\frac{\bar{p}_{\rm s}\Omega_{\rm r}+N_0+4p_{\rm u}\wp}{p_{\rm s}\Omega_{\rm r}+N_0+4p_{\rm u}\wp})}{2\ln(2)\left(1+1/\chi(\bar{p}_{\rm s})\right)}-1\geq\frac{\mathcal{R}_{th}}{B}. \tag{22b}$$

Given the required number of iteration M to reach the convergence, the computational complexity of solving problem in (22) through CVX tools can be calculated as $\mathcal{O}(M)$.

IV. Automatic Radar Signal Cancellation

For further performance improvement and comparison purposes, we consider the use of an auto-canceling radar signal

$$F_{\gamma^\star}(x)=\begin{cases}1-\sum_{l=1}^{L}\binom{L}{l}(-1)^{l-1}\frac{1}{1+(x^2+x)l\theta}\exp\left(-\frac{lN_0}{p_{\rm u}\Omega_{\rm c}}(x^2+x)\right), & X=X_1, \quad (9a)\\ 1-\sum_{l=0}^{L-1}\sum_{q=0}^{l}\frac{\binom{l}{q}q!(N_0)^{l-q}(p_{\rm s}\Omega_{\rm r})^q}{l!(\theta(x^2+x)\ +1)^{q+1}}\left(\frac{x^2+x}{p_{\rm u}\Omega_{\rm c}}\right)^l\exp\left(-\frac{N_0(x^2+x)}{p_{\rm u}\Omega_{\rm c}}\right), & X=X_2. \quad (9b)\end{cases}$$

model at the BS [3]. Specifically, its transmitting antenna inverts the radar symbol every adjacent periods, for example, $x_{\rm r}$ for the period T and $-x_{\rm r}$ for $2T$, and the receiving antenna processes the signals every two periods $2T$. Under a single antenna reception, the combined signal at BS is given by

$$y = \sqrt{p_{\rm u}} h_{\rm c}\left(x_{\rm c}^1 + x_{\rm c}^2\right) + \sqrt{\beta} x_{\rm b}\sqrt{p_{\rm u}} h_{\rm b}\left(x_{\rm c}^1 + x_{\rm c}^2\right) + n_{2T}, \quad (23)$$

where $x_{\rm c}^t$ $(t = 1, 2)$ is the symbol of UE at the t-th period such that $\mathbb{E}\{|x_{\rm c}^t|\} = 0$ and $\mathbb{E}\{|x_{\rm c}^t|^2\} = 1$ while $n_{2T} \sim \mathcal{CN}(0, 2N_0)$.

For this auto-interference cancellation model, the minimal SINR for symbiotic communication at BS converges to $\gamma = \min\{p_{\rm u}X/[\beta p_{\rm u}Y + N_0], \beta p_{\rm u}Y/N_0\}$. Considering the backscattering coefficient adaptively (akin to Proposition 1), we can derive the maximal SINR and OP respectively as

$$\gamma^\star = \left(\sqrt{1 + 4p_{\rm u}X/N_0} - 1\right)/2, \quad (24)$$

$$\text{OP} = \Pr(C(\gamma^\star) \le R_m) = F_X\left(N_0\left(2^{4R_m} - 2^{2R_m}\right)/p_{\rm u}\right). \quad (25)$$

Once the symbiotic communication signals are decoded, the radar signal is processed by subtracting them within one period, such as T, and retains the structure $y_{\rm rad} = \sqrt{p_{\rm s}} h_{\rm r} x_{\rm r} + n$. As a result, the radar mutual information is given by (13).

It is worth noting that this auto-interference cancellation model effectively restores pure symbiotic communication signals and maximizes radar mutual information, regardless of the radar transmission power level. However, it requires phase-shift designs in modulation [3] to prevent the occurrence of two symbols with opposite polarities during signal detection.

V. Numerical Results and Discussion

This section presents numerical results for the SymCom performance and radar sensing activity when $\Omega_{\rm c} = 0.5$, $\Omega_{\rm u} = 0.4$, $\Omega_{\rm b} = 0.3$, $\Omega_{\rm r} = 0.2$, $N_0 = 1$, and $B = 1$ MHz.

Fig. 2(a) shows the OP performance, OP, versus the UE transmission power under target rate $R_m = 0.5$ [bps/Hz]. One can observe that the OP decreases as $p_{\rm u}$ increases and that the asymptotic OPs using (10) are fairly close to the exact value. Compared to fixed backscattering coefficient $\beta = 0.1, 0.5$, the adaptive solution $\beta^\star$ from Proposition 1 significantly reduces the OP, especially at high $p_{\rm u}$. Besides, the non-auto-canceling radar signal model (non-auto) outperforms the auto-canceling model due to reduced decoding time, leading to fewer outage events. Besides, for the diversity approaches, SC yields a higher OP than the beamforming-based MRC strategy, confirming Remark 1. On the other hand, Fig. 2(b) shows that no OP improvement occurs with $\beta = 0.1$, but for $\beta^\star$, increasing the number of antennas L widens the OP gap between SC and beamforming-based MRC strategies.

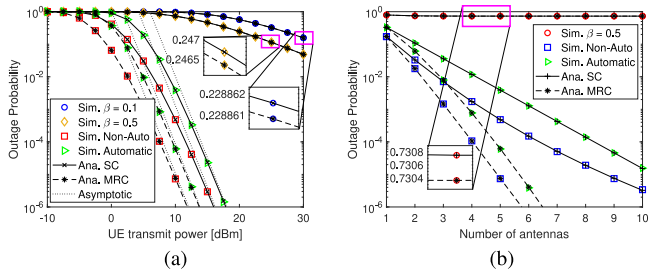

(a) (b)

Fig. 2. OP of SymCom: a) Impact of UE's transmission power $p_{\rm u}$ at $L = 5$ and b) Impact of number of antenna L at $p_{\rm s} = 5$ [dBm].

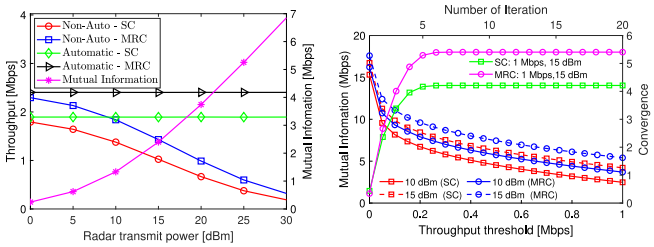

(a) (b)

Fig. 3. Mutual information of radar sensing: a) Impact of radar transmission power $p_{\rm s}$ and b) Impact of throughput threshold $\mathcal{R}_{th}$.

Given $L = 5$, Fig. 3(a) illustrates the relationship between throughput and radar mutual information at $\mathcal{R}_{th} = 0.5$ Mbps and $p_{\rm u} = 10$ dBm. This figure highlights that a performance trade-off in non-auto-canceling radar signal models: while increasing the radar transmission power $p_{\rm s}$ enhances radar mutual information, it also decreases the throughput, as noted in Remark 1. In contrast, the throughput in the auto-canceling signal model remains stable due to no interference from radar signals. Fig. 3(b) clearly demonstrates the effectiveness of our proposed solution for maximizing mutual information. Our approach decisively minimizes the number of iterative searches required to achieve convergence, managing to reach this goal

$$\Xi(\bar{p}_{\rm s}) = \begin{cases} 1 + \sum_{l=1}^{L} \frac{\binom{L}{l}(-1)^{l-1}}{\ln(2)} \sum_{k=1}^{K} \frac{\pi\sqrt{1-\phi_k^2}}{4K} \frac{\exp\left(-\frac{lN_0}{4p_{\rm u}\Omega_{\rm c}}(2\tau_k - 1)/(1-\tau_k)^2\right)}{(1-\tau_k)(1 + l\theta(2\tau_k - 1)/(1-\tau_k)^2/4)}, & X = X_1, \quad (20a) \\ 1 + \sum_{l=0}^{L-1}\sum_{q=0}^{l} \frac{\binom{l}{q} q!(\Omega_{\rm r} p_{\rm s})^q}{l!\ln(2)(N_0)^{q-l}} \sum_{k=1}^{K} \frac{\pi\sqrt{1-\phi_k^2}}{4K} \frac{\left(\frac{2\tau_k - 1}{4p_{\rm u}\Omega_{\rm c}(1-\tau_k)^2}\right)^l \exp\left(-\frac{N_0(2\tau_k-1)}{4p_{\rm u}\Omega_{\rm c}(1-\tau_k)^2}\right)}{(1-\tau_k)(1 + \theta(2\tau_k - 1)\ /(1-\tau_k)^2/4)^{q+1}}, & X = X_2, \quad (20b) \end{cases}$$

$$\chi(\bar{p}_{\rm s}) = \begin{cases} 1 + \sum_{l=1}^{L} \binom{L}{l}(-1)^{l-1} \sum_{k=1}^{K} \frac{\pi\sqrt{1-\phi_k^2}}{4K} \frac{\exp\left(-\frac{lN_0}{4p_{\rm u}\Omega_{\rm c}}(\tau_k^2/(1-\tau_k)^2 - 1)\right)}{(1-\tau_k)^2 + l\theta(2\tau_k - 1)/4}, & X = X_1, \quad (21a) \\ 1 + \sum_{l=0}^{L-1}\sum_{q=0}^{l} \frac{\binom{l}{q} q!(\Omega_{\rm r} p_{\rm s})^q}{l!(N_0)^{q-l}} \sum_{k=1}^{K} \frac{\pi\sqrt{1-\phi_k^2}}{4K} \frac{\left(\frac{2\tau_k - 1}{4p_{\rm u}\Omega_{\rm c}(1-\tau_k)^2}\right)^l \exp\left(-\frac{N_0(2\tau_k-1)}{4p_{\rm u}\Omega_{\rm c}(1-\tau_k)^2}\right)}{(\theta(2\tau_k - 1)\ /(1-\tau_k)^2/4 + 1)^{q+1}(1-\tau_k)^2}, & X = X_2. \quad (21b) \end{cases}$$

within just 6 iterations for both SC and MRC at the specified throughput threshold of $\mathcal{R}_{th} = 1$ Mbps. Furthermore, our method robustly adapts to increases in $\mathcal{R}_{th}$, ensuring that the transmission power for radar sensing steadily increases to maintain throughput above the threshold. However, it is crucial to note that as $\mathcal{R}_{th}$ continues to rise, a lower power assignment is necessary to ensure the throughput condition, resulting in a downward trend in mutual information.

VI. Conclusion

The SaSC systems' sensing and symbiotic communication performances were analyzed under adaptive backscattering coefficient configurations and diversity techniques, followed by the problem of mutual information maximization aware of throughput above the acceptable threshold, and finally, radar signal auto-cancellation models. Numerical simulations demonstrated the transformative potential of the proposed SaSC approach in integrated systems.

Appendix A
Proof of Lemma 1

For $X = X_1$, we apply the binominal theorem in [12, (1.111)] for (7b) and then replace it and (8) into (6) to get

$$F_{\gamma^\star}(x) = 1 - \sum_{l=1}^{L} \binom{L}{l} \frac{(-1)^{l-1}}{\Omega_{\rm r}} \exp\left(-lN_0 \frac{\left(x^2+x\right)}{p_{\rm u}\Omega_{\rm c}}\right) \times \int_0^\infty \exp\left(-lp_{\rm s} z \frac{\left(x^2+x\right)}{p_{\rm u}\Omega_{\rm c}} - \frac{z}{\Omega_{\rm r}}\right) dz. \quad (26)$$

For $X = X_2$, we use the incomplete Gamma property in [12, (8.352.4)] for (7b) and then replace it and (8) into (6) to get

$$F_{\gamma^\star}(x) = 1 - \sum_{l=0}^{L-1} \sum_{q=0}^{l} \frac{\binom{l}{q}(N_0)^{l-q}(p_{\rm s})^q}{l!\Omega_{\rm r}} \left(\frac{\left(x^2+x\right)}{p_{\rm u}\Omega_{\rm c}}\right)^l \exp\left(-\frac{N_0\left(x^2+x\right)}{p_{\rm u}\Omega_{\rm c}}\right) \int_0^\infty z^q \exp\left(-p_{\rm s} z \frac{\left(x^2+x\right)}{p_{\rm u}\Omega_{\rm c}} - \frac{z}{\Omega_{\rm r}}\right) dz. \quad (27)$$

Finally, we make use of [12, (3.326.2)] for (26) and (27), we get the respective solutions in (9a) and (9b).

Appendix B
Proof of Equation (17)

Over the domain $x, y > 0$, $g(x,y) = \log_2(1 + 1/\sqrt{xy})$ is a convex function, and thus, the first-order optimality condition can be applied for $(\bar{x}, \bar{y})$, i.e., $g(\bar{x},\bar{y}) + < \bigtriangledown g(\bar{x},\bar{y}), (x,y) - (\bar{x},\bar{y}) >$, to have the following inequality

$$g(x,y) \geq g(\bar{x},\bar{y}) + \frac{1}{2\ln(2)(1+\sqrt{\bar{x}\bar{y}})}\left(2 - \frac{x}{\bar{x}} - \frac{y}{\bar{y}}\right). \quad (28)$$

Mapping $y = 1/(x+c)$ and $\bar{y} = 1/(\bar{x}+c)$ yields the outcome.

Appendix C
Proof of Equations (20) and (21)

We start this proof by first deriving $F_U(u) = \Pr(U < u)$. For $u < 1$, we can get that $F_U(u) = 0$, which leads to

$$\Xi(\bar{p}_{\rm s}) = \frac{1}{\ln(2)} \int_0^1 \frac{du}{1+u} = 1, \; \chi(\bar{p}_{\rm s}) = \int_0^1 du = 1. \quad (29)$$

For $u \geq 1$, we can get that

$$F_U(u) = \int_0^\infty F_X\left((\bar{p}_{\rm s} z + N_0)\frac{(u^2-1)}{4p_{\rm u}}\right) f_Z(z)\, dz, \quad (30)$$

which has the same form with (6). Following that, we can rely on (9) to derive $\Xi(\bar{p}_{\rm s})$ and $\chi(\bar{p}_{\rm s})$ by replacing $(x^2+x)/p_{\rm u}$ with $(u^2-1)/[4p_{\rm u}]$. However, to the best of the authors' knowledge, there is no further closed-form for the outcomes of $\Xi(\bar{p}_{\rm s})$ and $\chi(\bar{p}_{\rm s})$; thus, we propose to tackle this problem using the variable exchange $u = y/(1-y)$ before employing the Gauss-Chebyshev Quadrature method [13, (45)].

Finally, putting (29) and the results of $\Xi(\bar{p}_{\rm s})$ and $\chi(\bar{p}_{\rm s})$ subject to $u \geq 1$ together, we attain (20) and (21).

References

[1] F. Liu et al., "Integrated sensing and communications: Toward dual-functional wireless networks for 6G and beyond," *IEEE J. Sel. Areas Commun.*, vol. 40, no. 6, pp. 1728–1767, Jun. 2022.

[2] Z. Wei et al., "Integrated sensing and communication channel modeling: A survey," *IEEE Internet Things J.*, vol. 12, no. 12, pp. 18850–18864, Jun. 2025.

[3] H. Liu and E. Alsusa, "A novel ISaC approach for uplink NOMA system," *IEEE Commun. Lett.*, vol. 27, no. 9, pp. 2333–2337, Sep. 2023.

[4] Z. Yu et al., "Addressing the mutual interference in uplink ISAC receivers: A projection method," *IEEE Wireless Commun. Lett.*, vol. 13, no. 11, pp. 3109–3113, Nov. 2024.

[5] C. Ouyang, Y. Liu, and H. Yang, "On the performance of uplink ISAC systems," *IEEE Commun. Lett.*, vol. 26, no. 8, pp. 1769–1773, Aug. 2022.

[6] C. Ouyang, Y. Liu, and H. Yang, "Performance of downlink and uplink integrated sensing and communications (ISAC) systems," *IEEE Wireless Commun. Lett.*, vol. 11, no. 9, pp. 1850–1854, Sep. 2022.

[7] Z. Wang et al., "Symbiotic sensing and communications towards 6G: Vision, applications, and technology trends," in *Proc. IEEE Veh. Technol. Conf.*, Sep. 2021, pp. 1–5.

[8] A. Hakimi, S. Zargari, and C. Tellambura, "Integrated communication and sensing with symbiotic radio and RIS-assisted backscatter," *IEEE Wireless Commun. Lett.*, vol. 14, no. 1, pp. 38–42, Jan. 2025.

[9] Q. Tao, X. Hu, S. Zhang, and C. Zhong, "Integrated sensing and communication for symbiotic radio systems in mobile scenarios," *IEEE Trans. Wireless Commun.*, vol. 23, no. 9, pp. 11213–11225, Sep. 2024.

[10] Q. Tao, C. Huang, and X. Chen, "Integrated sensing and communication for symbiotic radio with multiple IoT devices," *IEEE Commun. Lett.*, vol. 28, no. 8, pp. 1820–1824, Aug. 2024.

[11] F. Xia et al., "Symbiotic sensing and communication: Framework and beamforming design," *IEEE Trans. Wireless Commun.*, vol. 24, no. 3, pp. 2417–2434, Mar. 2025.

[12] I. S. Gradshteyn and I. M. Ryzhik, *Table of Integrals, Series, and Products*. Cambridge, MA, USA: Academic, 2014.

[13] T.-H. Vu, T.-V. Nguyen, and S. Kim, "Cooperative NOMA-enabled SWIPT IoT networks with imperfect SIC: Performance analysis and deep learning evaluation," *IEEE Internet Things J.*, vol. 9, no. 3, pp. 2253–2266, Feb. 2021.